mater.scichina.com link.springer.com

Published online 2 February 2021 | https://doi.org/10.1007/s40843-020-1566-6
Sci China Mater 2021, 64(7): 1662–1670

Highly efficient oxygen evolution and stable water splitting by coupling NiFe LDH with metal phosphides

Chengye Song[1,2†], Yi Liu[1†], Yuchao Wang[1,4†], Shuaihao Tang[1,5], Wenkui Li[2*], Qian Li[1,4], Jian Zeng[1,5], Lei Chen[3], Hongcheng Peng[3] and Yongpeng Lei[1,3,6*]

ABSTRACT **It is a great challenge to develop highly active oxygen evolution reaction (OER) electrocatalysts with superior durability. In this study, a NiFe layered double hydroxide-decorated phosphide (NiFe LDH@CoP/NiP_3) was constructed to display satisfactory OER activity and good stability for water splitting in alkaline media. At an overpotential of 300 mV, NiFe LDH@CoP/NiP_3 achieved a current density of 82 mA cm^{-2} for the OER, which was 9.1 and 2.3 times that of CoP/NiP_3 and NiFe LDH, respectively. Moreover, the reconstruction behavior, during which oxyhydroxides formed, was studied by a combination of X-ray photoelectron spectroscopy, Raman spectroscopy, and scanning electron microscopy. A synergistic effect between NiFe LDH and CoP/NiP_3 was also observed for the hydrogen evolution reaction. Furthermore, when NiFe LDH@CoP/NiP_3 acted as both the cathode and anode for overall water splitting, a high current density of 100 mA cm^{-2} was maintained for more than 275 h. In addition, under Xe light irradiation, a solar-to-hydrogen efficiency of 9.89% was achieved for solar-driven water splitting. This work presents the coupling of different active compositions, and can provide a reference for designing bifunctional electrocatalysts.**

Keywords: bifunctional electrocatalysis, oxygen evolution reaction, phosphides, layered double hydroxides, water splitting

INTRODUCTION

Efficient electrocatalytic overall water splitting is expected to alleviate the increasingly severe energy shortage and environmental crisis [1–4]. However, the slow kinetics of the oxygen evolution reaction (OER) and poor durability of catalysts under alkaline conditions [5–8]. Although RuO_2, IrO_2 and others have been utilized, there is an urgent necessity to develop earth-abundant OER catalysts with high activity, good stability, and low cost [9–12]. In previous studies, a series of OER catalysts in alkaline solutions have been developed, including metal oxides [13,14], hydroxides [15], selenides [16], sulfides [17,18], carbides [19], phosphides [20,21], and others [22–24]. Although phosphides generally show good hydrogen evolution reaction (HER) activity because of their similar catalytic mechanism to that of hydrogenase [25], their OER activities are unsatisfactory. Additionally, during the OER, phosphides are usually converted to oxyhydroxides, which are considered to be real active sites [26]. The investigation of reconstruction behavior requires more attention [27].

In contrast, layered double hydroxides (LDHs) are regarded as excellent OER catalyst candidates [28,29]. They have large specific surface areas and porous structures, which are beneficial for increasing the number of active sites and promoting mass transfer. However, because of their weak hydrogen adsorption, LDHs exhibit relatively poor HER activity, thus hindering their potential as bifunctional OER/HER catalysts. Synergistic effects play important roles in boosting bifunctional performance, such as in the OER/HER [30]. Yang *et al.* [31] decorated LDH with $CoNiSe_2$ to adjust H_2O chemisorption and

[1] State Key Laboratory of Powder Metallurgy, Central South University, Changsha 410083, China
[2] School of Materials and Mechanical Engineering, Jiangxi Key Laboratory of Surface Engineering, Jiangxi Science and Technology Normal University, Nanchang 330013, China
[3] Hunan Provincial Key Laboratory of Chemical Power Sources, College of Chemistry and Chemical Engineering, Central South University, Changsha 410083, China
[4] School of Material Science and Engineering, Central South University of Forestry and Technology, Changsha 410004, China
[5] Energy Materials Computing Center, Jiangxi University of Science and Technology, Nanchang 330013, China
[6] State Key Laboratory of Advanced Chemical Power Sources, Guizhou Meiling Power Sources Co. Ltd., Zunyi 563003, China
† These authors contributed equally to this work.
* Corresponding authors (emails: lypkd@163.com (Lei Y); liwenkui1976@163.com (Li W))

produce reactive H intermediates, thus leading to efficient overall water splitting. Liang *et al.* [32] electrodeposited amorphous NiFe hydroxides onto a NiFeP surface to construct a hybrid structure. The resulting electronic interactions boosted water oxidation by lowering the adsorption energy of H_2O. Thus, it could be proposed that metal phosphides and NiFe LDH may compensate each other's weaknesses when combined, achieving bifunctional OER/HER activity [33,34].

In this study, we coupled NiFe LDH with metal phosphides to boost the OER activity and stability of water splitting in alkaline media. For the OER, at an overpotential of 300 mV, NiFe LDH@CoP/NiP_3 achieved a current density of 82 mA cm^{-2}, which was 9.1 and 2.3 times that of CoP/NiP_3 and NiFe LDH, respectively. The reconstruction behavior during the OER was also studied. As both the cathode and anode in an electrolytic cell, NiFe LDH@CoP/NiP_3, demonstrated robust stability for 275 h at a high current density of 100 mA cm^{-2}. Using the simulated solar illumination, water splitting driven by solar cells achieved a solar-to-hydrogen (STH) efficiency of 9.89%.

EXPERIMENTAL SECTION

Materials

$Fe(NO_3)_3{\cdot}9H_2O$, $Ni(NO_3)_2{\cdot}6H_2O$, $CO(NH_2)_2$, $NaH_2PO_2{\cdot}H_2O$ and NH_4F were purchased from Sinopharm Chemical Reagent Co, Ltd. (SCRC). $Co(NO_3)_2{\cdot}6H_2O$ and $C_3H_4N_2$ were purchased from Shanghai Macklin Biochemical Co, Ltd. All the reagents were of analytical grade and used directly without further purification.

Preparation of the catalysts

Synthesis of CoP/NiP_3

Firstly, $Co(NO_3)_2{\cdot}6H_2O$ (1 mmol), NH_4F (5 mmol) and $CO(NH_2)_2$ (5 mmol) were mixed and dissolved in 30 mL deionized (DI) water. Before hydrothermal reaction, Ni foams were successively cleaned with 3 mol L^{-1} HCl, ethanol, and pure water under ultrasonication for 15 min to remove surface oxides and impurity. The mixture and a piece of Ni foam (2 × 1 cm^2) were shifted to Teflon-lined stainless-steel autoclave and warmed up to 120°C and maintained for 8 h. The precursor was washed with DI water and ethanol for three times and dried in vacuum at 60°C. Secondly, $C_3H_4N_2$ (0.30 g) and the as-prepared precursor were put on the upper and downstream of quartz boat, respectively. Then the obtained sample was calcined to 280°C (2°C min^{-1}) and maintained for 2 h in N_2. Next, phosphorization was realized at 260°C under the condition of the second step except using $NaH_2PO_2{\cdot}H_2O$.

Synthesis of NiFe LDH@CoP/NiP_3

The synthesis of NiFe LDH was referred to literature [34]. $Fe(NO_3)_3{\cdot}9H_2O$ (0.25 mmol), $Ni(NO_3)_2{\cdot}6H_2O$ (0.75 mmol) and $CO(NH_2)_2$ (1.25 mmol) were mixed and dissolved in 30 mL DI water. The mixture and the above CoP/NiP_3 (2 × 1 cm^2) were shifted to a Teflon-lined stainless-steel autoclave and warmed up to 120°C and maintained for 10 h. The sample was washed with DI water and ethanol for three times and dried in vacuum at 60°C.

Synthesis of NiFe LDH

NiFe LDH was synthesized by the similar process as NiFe LDH@CoP/NiP_3. $Fe(NO_3)_3{\cdot}9H_2O$ (0.25 mmol), $Ni(NO_3)_2{\cdot}6H_2O$ (0.75 mmol) and $CO(NH_2)_2$ (1.25 mmol) were mixed and dissolved in 30 mL DI water. Then, the mixture and a piece of treated Ni foam (2 × 1 cm^2) instead of CoP/NiP_3 were shifted to a Teflon-lined stainless-steel autoclave and warmed up to 120°C and maintained for 10 h. The sample was washed with DI water and ethanol for three times and dried in vacuum at 60°C.

Characterizations

The crystalline structures were tested by X-ray diffraction (XRD) on D/max 2550 VB with 40 kV and Cu Kα radiation (λ = 1.5418 Å). The morphology of the samples was characterized by a field emission scanning electron microscope (FE-SEM, Quanta 250 FEG) and transmission electron microscope (FE-TEM, FEI Tecnai G2 F20). X-ray photoelectron spectroscopy (XPS) measurements were performed on Thermo Fisher Scientific K-Alpha with a monochromatic Al-Kα X-ray source. All XPS spectra were calibrated by shifting the detected adventitious C 1s peak to 284.4 eV. Raman spectra were measured by the Horibajylabram HR Evolution with a 532-nm excitation laser.

Electrochemical test

OER and HER tests were performed in a three-electrode system of an electrochemical station (CHI 660E) at room temperature. A graphite rod and a saturated calomel electrode (SCE) were used as the counter electrode and the reference electrode, respectively. The prepared NiFe LDH@CoP/NiP_3 was directly used as the work electrode without further treatment. The reference electrode is converted into a potential relative to the reversible hydrogen electrode (RHE): E(RHE) = E(SCE) + 0.2415 +

0.0591 × pH. The water splitting was conducted in 1 mol L^{-1} KOH through a two-electrode system which employed NiFe LDH@CoP/NiP_3 as both cathode and anode. All the linear sweep voltammetry (LSV) of HER, OER and water splitting were tested at the sweep rate of 2 mV s^{-1} with 90% internal resistance (IR) compensation.

For the solar-driven water splitting, the STH efficiency can be defined as the following equation:

STH (%) = Chemical energy output/Solar energy input $= j \times A \times E_f \times FE_{H_2}/(P_s \times A)$,

where j represents the operating current density; A represents the effective illuminated area; E_f is the standard thermodynamic potential difference between HER and OER (1.23 V). FE_{H_2} is the Faradic efficiency of HER which is regarded as 100%; P_s is the power of simulated solar illumination (100 mW cm^{-2}).

RESULTS AND DISCUSSION

To realize the composite of CoP/NiP_3 and NiFe LDH, CoP/NiP_3 was synthesized, followed by the growth of NiFe LDH (Fig. S1). The specific quantities of raw materials are stated in Table S1. XRD patterns were recorded to obtain crystallographic information (Fig. 1a). Table S2 summarizes the peaks for NiFe LDH@CoP/NiP_3 and their attributions. The peaks located at 2θ = 45.1°, 52.3° and 76.8° correspond to the (111), (200), and (220) crystallographic planes of metallic Ni (PDF#03-1051), respectively. The peaks at 2θ = 21.4° and 39.4° indicate the presence of nickel hydroxides (PDF#73-1520). The peak at 2θ = 36.1° corresponds to the (111) crystallographic plane of CoP (PDF#29-0497). The peaks at 16.0° and 36.3° correspond to the (200) and (013) crystallographic planes of NiP_3 (PDF#73-1242), respectively. XPS was then conducted to determine the surface composition and chemical valence (Figs S2–S7). As shown in Fig. 1b, NiFe LDH@CoP/NiP_3 presents peaks corresponding to Fe, Co, Ni, C, P and O. The coexistence of Fe and P illustrates that NiFe LDH@CoP/NiP_3 was successfully obtained. The element contents are stated in Table S3. We noted that the Fe content was only 0.1 wt%, which may suggest the low NiFe LDH content. Due to the low contents of Fe and Ni in the raw materials, the relative content of NiFe LDH was low; this explains the lack of recognizable characteristic peaks associated with NiFe LDH in the XRD patterns. Additionally, a weak peak at 26.6°, attributed to amorphous carbon, was observed, which resulted from small quantities of $CO(NH_2)_2$ and $C_3H_4N_2$ in the raw materials [35,36].

In the SEM images (Fig. 2a and Fig. S8), NiFe LDH@CoP/NiP_3 shows an arborized structure (a typical characteristic of metal phosphides) on Ni foam. This structure could facilitate intimate contact between the catalyst and electrolyte to boost the OER kinetics [37]. The energy dispersive spectra (EDS) of NiFe LDH@CoP/NiP_3 also supported the presence of Fe, Co, Ni, C, P, etc. (Fig. S9), in accordance with the XPS spectra. Furthermore, the uniform distribution of these elements was confirmed by the TEM elemental mapping images (Fig. 2b, c). Fig. 2d presents the morphology of NiFe LDH@CoP/NiP_3. The phosphides were decorated with thin LDH nanosheets. The high-resolution TEM images (Fig. 2e, f) show the presence of CoP and NiP_3 particles. The clear crystal planes with d-spacing of 0.248 and 0.208 nm correspond to the (111) plane of CoP and the (321) plane of NiP_3, respectively.

The OER performance was evaluated in 1 mol L^{-1} KOH solution (Fig. 3a). As shown, NiFe LDH@CoP/NiP_3 only required an overpotential of 239 mV to drive 10 mA cm^{-2}, outperforming its isolated NiFe LDH and CoP/NiP_3 counterparts [38]. At a large current density of 100 mA cm^{-2}, NiFe LDH@CoP/NiP_3 also displayed a significant overpotential advantage (310 mV) compared

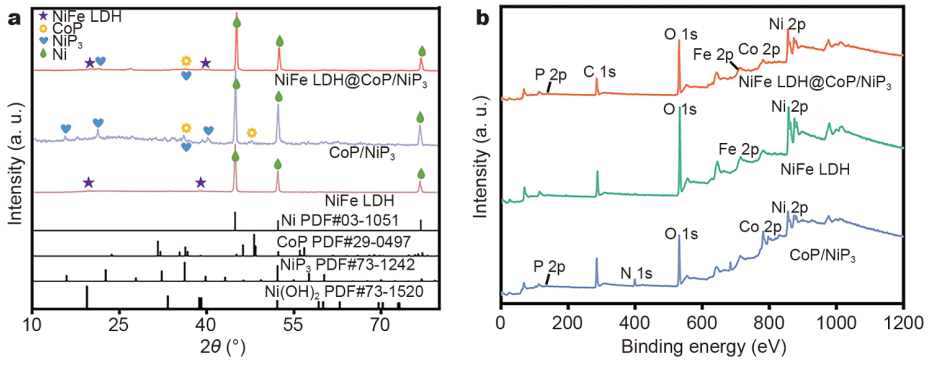

Figure 1 (a) XRD patterns and (b) XPS survey of various samples.

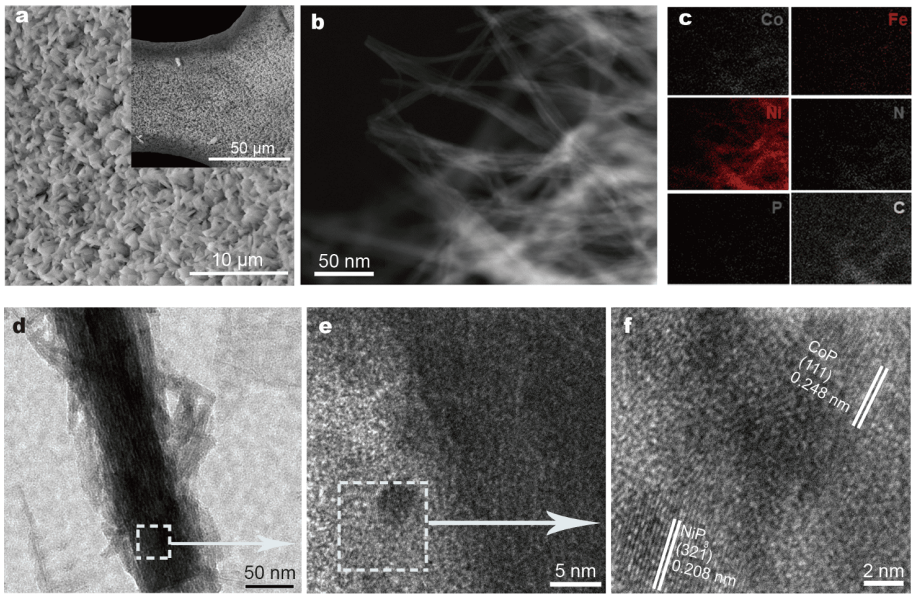

Figure 2 (a) SEM images of NiFe LDH@CoP/NiP_3. (b) TEM and (c) corresponding elemental mapping images. (d) TEM and (e, f) high-resolution TEM images of NiFe LDH@CoP/NiP_3.

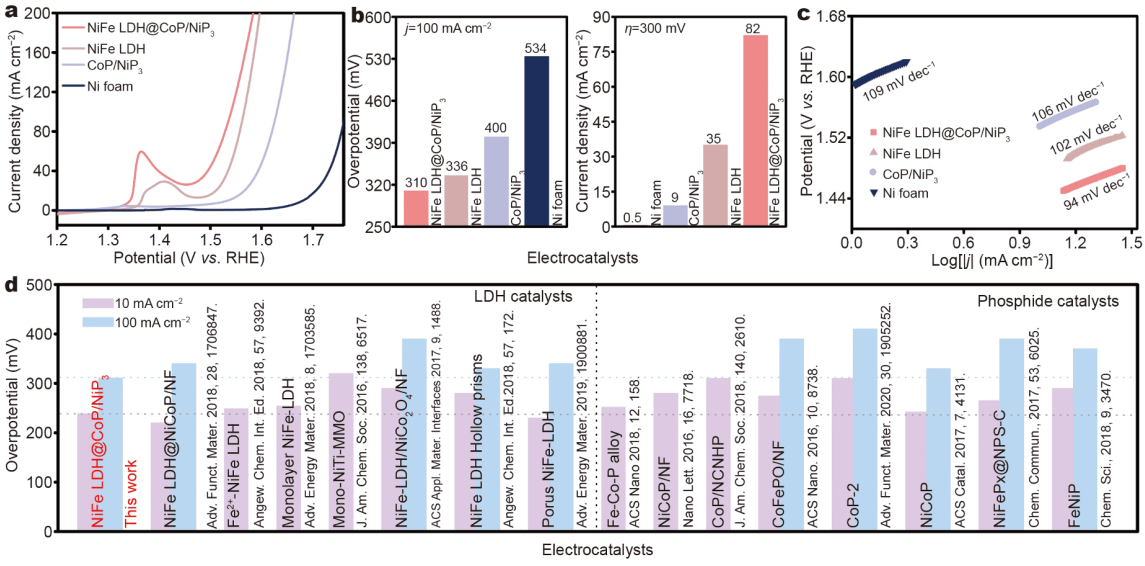

Figure 3 (a) OER polarization curves in 1.0 mol L^{-1} KOH. (b) Overpotentials at 100 mA cm^{-2} (left) and current densities at η = 300 mV (right) of different samples. (c) Tafel plots of different samples. (d) The overpotentials of recently reported electrocatalysts in 1.0 mol L^{-1} KOH.

with NiFe LDH and CoP/NiP_3. In particular, NiFe LDH@CoP/NiP_3 only required an overpotential of 300 mV to reach a current density of 82 mA cm^{-2}, which is 164.0, 9.1 and 2.3 times that of Ni foam, CoP/NiP_3 and NiFe LDH, respectively (Fig. 3b). The Tafel slope value of NiFe LDH@CoP/NiP_3 was 94 mV dec^{-1} (Fig. 3c), which indicates faster kinetics than the other samples [39]. Based on the above result, the enhanced OER activity should be attributed to the synergy of CoP/NiP_3 and NiFe LDH [40]. Compared with both LDH catalysts and phosphide catalysts reported recently, NiFe LDH@CoP/NiP_3 exhibited a relatively favorable performance at both 10 and 100 mA cm^{-2} (Fig. 3d and Tables S4 and S5). The NiFe LDH@CoP/NiP_3 demonstrated good stability for

more than 70 h at an overpotential of 300 mV (Fig. S10).

It has been reported that phosphides exhibit self-reconstruction phenomena during the OER process [41–43]. The reconstructed catalysts, with oxyhydroxides on the surface, inherit the advantages of nanostructures, which are stable and act as the true active species [40]. To investigate the reconstruction of NiFe LDH@CoP/NiP_3 during OER, XPS and Raman spectra were recorded before and after OER. In Fig. 4a, the Co $2p_{3/2}$ peaks at 774.8, 780.3 and 796.4 eV correspond to the Co^0, oxidized Co^{2+}/Co^{3+}, and satellite peak, respectively [44]. The weakened Co^0 peak of NiFe LDH@CoP/NiP_3 after OER indicates the improved oxidation state of the Co species. As shown in Fig. 4b, the binding energies of Ni $2p_{3/2}$ (854.9 eV) and Ni $2p_{1/2}$ (872.7 eV) shift to 855.3 and 873.0 eV, respectively, demonstrating the improved oxidation state after OER [45]. In the O 1s spectra of NiFe LDH@CoP/NiP_3 (Fig. 4c), the peaks at 530.4 and 531.5 eV are attributed to M–O bonds (M representing metal) and oxygen defects in LDH, respectively. The peak at 532.5 eV corresponds to the adsorbed O resulting from hydroxyl groups (such as adsorbed H_2O) [46]. In the Raman spectra of NiFe LDH@CoP/NiP_3, the peaks located at 188, 321 and 534 cm^{-1} correspond to O–M–O, O–H and M–O–M vibrations in LDH, respectively (Fig. 4d and Table S6) [47–49]. After the OER, the peaks at 188 and 321 cm^{-1} were not present because of the conversion of hydroxides into oxyhydroxides. Under anodic potentials, the hydrophilic, conductive and chemically stable M–OOH may be formed. This could serve as the real active composition to boost OER activity [50–53]. The crystal structure and surface morphology of NiFe LDH@CoP/NiP_3 after OER were also investigated. After the OER process, the phosphide peak intensity was reduced, which may be attributed to the formation of amorphous oxyhydroxides. In the SEM images (Fig. S11a, b), the initial arborized structure was seen to have transformed into a finer flower-like structure after the OER. This change in surface morphology also confirmed the reconstruction of the catalyst, consistent with the afore-described XPS and Raman results. After reconstruction of the phosphides, the M–OOH active site was introduced, and the transformed flower-like structure exposes more active sites. These factors significantly improve the catalyst activity.

Subsequently, the HER activity of NiFe LDH@CoP/NiP_3 was evaluated, which demonstrated clear superiority over those of CoP/NiP_3 and NiFe LDH (Fig. 5a). The overpotentials of NiFe LDH@CoP/NiP_3 at different current densities are listed in Fig. S12. To reach a current density of 50 mA cm^{-2}, the required overpotential was only 206 mV (Fig. 5b left). For NiFe LDH@CoP/NiP_3, an

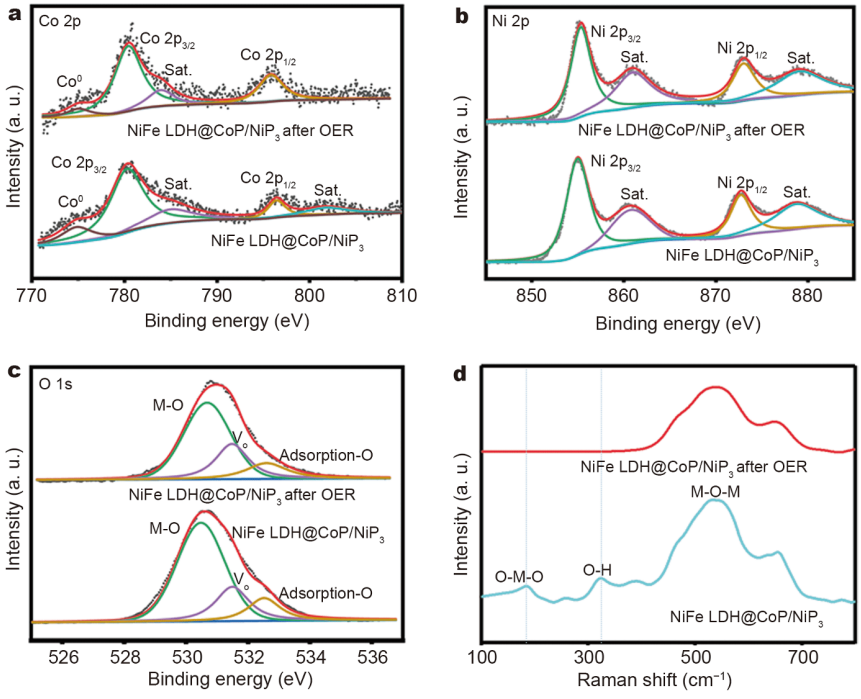

Figure 4 (a–c) The corresponding high-resolution XPS spectra of Co 2p, Ni 2p and O 1s. (d) Raman spectra of NiFe LDH@CoP/NiP_3.

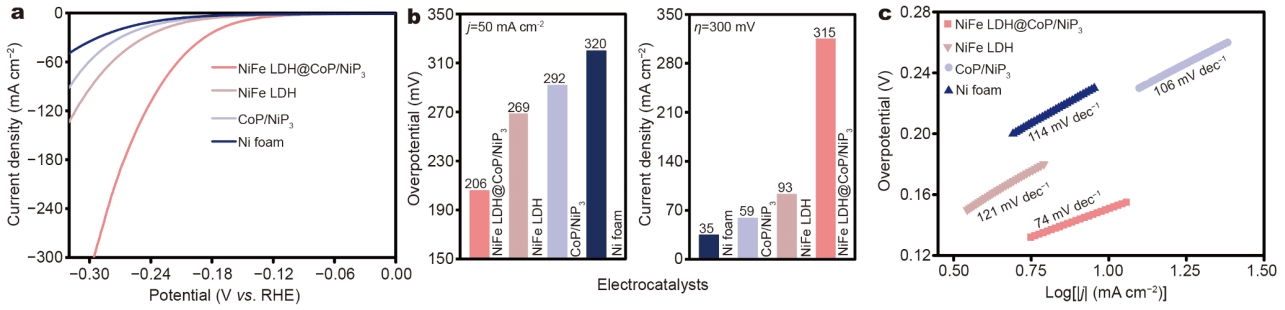

Figure 5 (a) HER polarization curves in 1.0 mol L^{-1} KOH. (b) Overpotentials at 50 mA cm^{-2} (left) and current densities at η = 300 mV (right) of various samples. (c) Tafel plots of different samples.

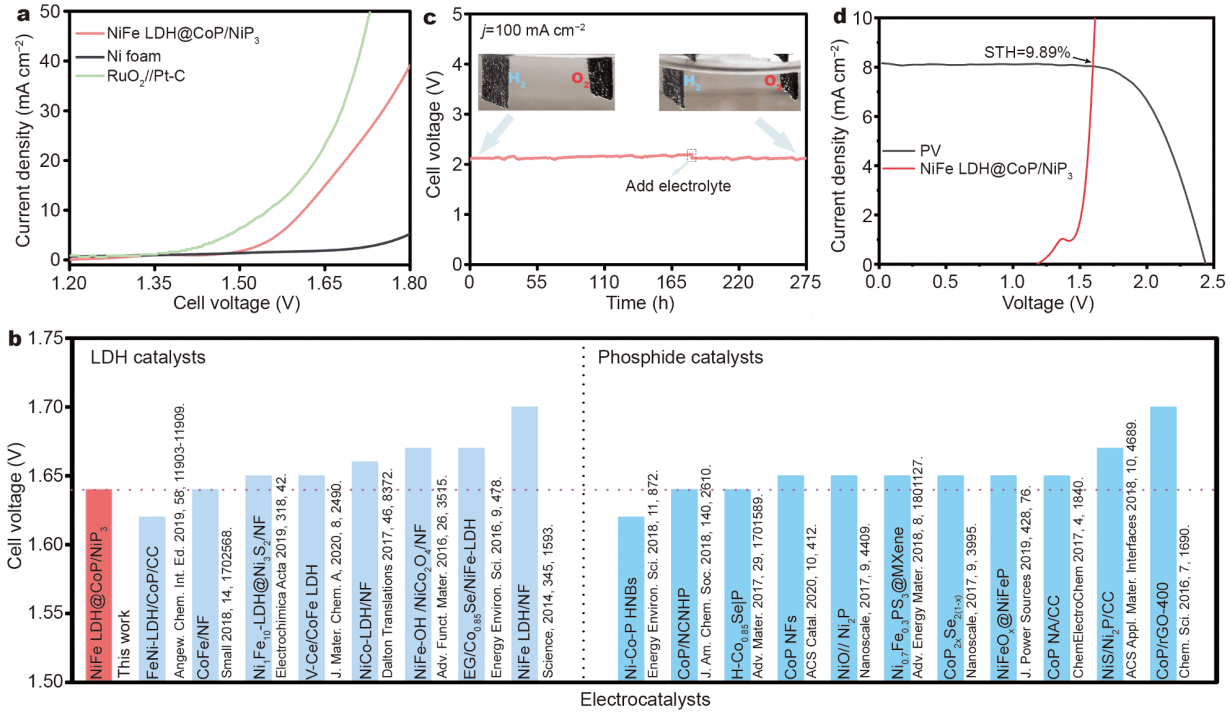

Figure 6 (a) Overall water splitting polarization curves in 1.0 mol L^{-1} KOH. (b) The required cell voltage of electrocatalysts at 10 mA cm^{-2} in recent years. (c) Stability test of NiFe LDH@CoP/NiP_3. Insets: photograph evolving from the electrodes at the beginning of stability test and after 275 h. (d) *J-V* curve of a solar cell and the polarization curve of NiFe LDH@CoP/NiP_3 for water splitting in a two-electrode system.

overpotential of 300 mV resulted in a current density of 315 mA cm^{-2}, which is 9.0, 5.3 and 3.4 times that of Ni foam, CoP/NiP_3, and NiFe LDH, respectively (Fig. 5b right). Fig. 5c shows that the Tafel slope of NiFe LDH@CoP/NiP_3 is also the smallest (74 mV dec^{-1}), indicating the Volmer-Heyrovsky mechanism [54].

Considering the above results, NiFe LDH@CoP/NiP_3 shows potential as a bifunctional OER/HER electrocatalyst. We then explored the overall water splitting performance (Fig. S13). Using NiFe LDH@CoP/NiP_3 as both the cathode and anode, a cell voltage of 1.64 V was required to reach a current density of 10 mA cm^{-2} (Fig. 6a), which is comparable to most of the reported results summarized in Fig. 6b, based on Tables S7 and S8. Notably, the constant current test at 100 mA cm^{-2} lasted for 275 h with negligible activity loss (Fig. 6c). As seen in the inset in Fig. 6c, H_2 bubbles at the cathode and the O_2 bubbles at the anode were continuously produced during the entire electrolysis process, further illustrating the excellent stability of the NiFe LDH@CoP/NiP_3 electrode. The high durability of this water splitting system undoubtedly makes it promising for application. We

speculated that, as a self-supporting electrode, the Ni foam achieved close contact with the catalyst layer, which reduced the charge transfer resistance and enhanced the durability under large current densities [55]. Additionally, the three-dimensional porous structure increased the area of exposed active sites, hence boosting the catalytic activity [56]. Then, we designed a simple solar-driven water splitting system, which comprised a commercial Si solar plane (16 cm^2) and electrodes. Fig. S14a, b show the electrolyzed water test, which used NiFe LDH@CoP/NiP_3 as both the cathode and anode in 1.0 mol L^{-1} KOH solution under Xe light irradiation as simulated sunlight. H_2 and O_2 were spontaneously produced under the simulated solar irradiation. From the current-voltage (*J-V*) curve of the solar cell and the polarization curve of the water splitting system, the operating current density at 1.59 V was calculated to be ~8 mA cm^{-2}, which corresponded to an STH efficiency of 9.89% (Fig. 6d) [57,58]. Thus, NiFe LDH@CoP/NiP_3 displayed potential to be used in solar-driven water splitting.

CONCLUSIONS

In summary, NiFe LDH@CoP/NiP_3 was constructed as a bifunctional OER/HER catalyst, which demonstrated improved performance over the sum of its isolated components. Under alkaline condition, NiFe LDH@CoP/NiP_3 achieved an OER current density of 82 mA cm^{-2} (at an overpotential of 300 mV), which was 9.1 times that of CoP/NiP_3. Moreover, the reconstruction behavior during the OER was studied. In particular, for overall water splitting, the sample displayed excellent durability for 275 h at 100 mA cm^{-2}. Under Xe light irradiation, the water splitting STH efficiency was 9.89%. A detailed study of the synergistic mechanism between CoP/NiP_3 and NiFe LDH is currently under way. This work presents the coupling of different active compositions and their synergistic catalytic performance, and can provide a reference for designing bifunctional electrocatalysts.

Received 25 August 2020; accepted 17 November 2020; published online 2 February 2021

1 Zhang M, Li X, Zhao J, *et al.* Surface/interface engineering of noble-metals and transition metal-based compounds for electrocatalytic applications. J Mater Sci Tech, 2020, 38: 221–236
2 Lei Y, Wang Y, Liu Y, *et al.* Designing atomic active centers for hydrogen evolution electrocatalysts. Angew Chem Int Ed, 2020, 59: 20794–20812
3 Zhang N, Ye C, Yan H, *et al.* Single-atom site catalysts for environmental catalysis. Nano Res, 2020, 13: 3165–3182
4 Chen Y, Ji S, Sun W, *et al.* Engineering the atomic interface with single platinum atoms for enhanced photocatalytic hydrogen production. Angew Chem Int Ed, 2020, 59: 1295–1301
5 Cai Z, Li L, Zhang Y, *et al.* Amorphous nanocages of Cu-Ni-Fe hydr(oxy)oxide prepared by photocorrosion for highly efficient oxygen evolution. Angew Chem Int Ed, 2019, 58: 4189–4194
6 Chen G, Zhu Y, Chen HM, *et al.* An amorphous nickel-iron-based electrocatalyst with unusual local structures for ultrafast oxygen evolution reaction. Adv Mater, 2019, 31: 1900883
7 Anantharaj S, Ede SR, Sakthikumar K, *et al.* Recent trends and perspectives in electrochemical water splitting with an emphasis on sulfide, selenide, and phosphide catalysts of Fe, Co, and Ni: A review. ACS Catal, 2016, 6: 8069–8097
8 Shang H, Sun W, Sui R, *et al.* Engineering isolated Mn–N_2C_2 atomic interface sites for efficient bifunctional oxygen reduction and evolution reaction. Nano Lett, 2020, 20: 5443–5450
9 Wang Q, Lei Y, Wang Y, *et al.* Atomic-scale engineering of chemical-vapor-deposition-grown 2D transition metal dichalcogenides for electrocatalysis. Energy Environ Sci, 2020, 13: 1593–1616
10 Yang J, Li W, Wang D, *et al.* Electronic metal-support interaction of single-atom catalysts and applications in electrocatalysis. Adv Mater, 2020, 32: 2003300
11 Dou Y, He CT, Zhang L, *et al.* Approaching the activity limit of $CoSe_2$ for oxygen evolution *via* Fe doping and Co vacancy. Nat Commun, 2020, 11: 1664
12 Liu Q, Wang Q, Wang J, *et al.* $TpyCo^{2+}$-based coordination polymers by water-induced gelling trigged efficient oxygen evolution reaction. Adv Funct Mater, 2020, 30: 2000593
13 Wang Q, Xue X, Lei Y, *et al.* Engineering of electronic states on Co_3O_4 ultrathin nanosheets by cation substitution and anion vacancies for oxygen evolution reaction. Small, 2020, 16: 2001571
14 Ling T, Zhang T, Ge B, *et al.* Well-dispersed nickel- and zinc-tailored electronic structure of a transition metal oxide for highly active alkaline hydrogen evolution reaction. Adv Mater, 2019, 31: 1807771
15 Liu R, Wang Y, Liu D, *et al.* Water-plasma-enabled exfoliation of ultrathin layered double hydroxide nanosheets with multivacancies for water oxidation. Adv Mater, 2017, 29: 1701546
16 Fang G, Wang Q, Zhou J, *et al.* Metal organic framework-templated synthesis of bimetallic selenides with rich phase boundaries for sodium-ion storage and oxygen evolution reaction. ACS Nano, 2019, 13: 5635–5645
17 Qin JF, Yang M, Chen TS, *et al.* Ternary metal sulfides MoCoNiS derived from metal organic frameworks for efficient oxygen evolution. Int J Hydrogen Energy, 2020, 45: 2745–2753
18 Zhang Y, Fu L, Shu Z, *et al.* Substitutional doping for aluminosilicate mineral and superior water splitting performance. Nanoscale Res Lett, 2017, 12: 456
19 Lei C, Zhou W, Feng Q, *et al.* Charge engineering of Mo_2C@defect-rich N-doped carbon nanosheets for efficient electrocatalytic H_2 evolution. Nano-Micro Lett, 2019, 11: 45
20 Zhang R, Tang C, Kong R, *et al.* Al-doped CoP nanoarray: a durable water-splitting electrocatalyst with superhigh activity. Nanoscale, 2017, 9: 4793–4800
21 You B, Sun Y. Innovative strategies for electrocatalytic water splitting. Acc Chem Res, 2018, 51: 1571–1580
22 Chen Z, Duan X, Wei W, *et al.* Boride-based electrocatalysts: emerging candidates for water splitting. Nano Res, 2020, 13: 293–314
23 Wang X, Vasileff A, Jiao Y, *et al.* Electronic and structural engineering of carbon-based metal-free electrocatalysts for water splitting. Adv Mater, 2019, 31: 1803625

24 Li X, Rong H, Zhang J, *et al.* Modulating the local coordination environment of single-atom catalysts for enhanced catalytic performance. Nano Res, 2020, 13: 1842–1855
25 Mishra IK, Zhou H, Sun J, *et al.* Hierarchical CoP/Ni_5P_4/CoP microsheet arrays as a robust pH-universal electrocatalyst for efficient hydrogen generation. Energy Environ Sci, 2018, 11: 2246–2252
26 Huang J, Li Y, Zhang Y, *et al.* Identification of key reversible intermediates in self-reconstructed nickel-based hybrid electrocatalysts for oxygen evolution. Angew Chem Int Ed, 2019, 58: 17458–17464
27 Cao J, Wang K, Chen J, *et al.* Nitrogen-doped carbon-encased bimetallic selenide for high-performance water electrolysis. Nano-Micro Lett, 2019, 11: 67
28 Zhang X, Zhao Y, Zhao Y, *et al.* A simple synthetic strategy toward defect-rich porous monolayer NiFe-layered double hydroxide nanosheets for efficient electrocatalytic water oxidation. Adv Energy Mater, 2019, 9: 1900881
29 Zhang Z, Zhou D, Zhou L, *et al.* NiFe LDH-CoPc/CNTs as novel bifunctional electrocatalyst complex for zinc–air battery. Ionics, 2018, 24: 1709–1714
30 Wu N, Lei Y, Wang Q, *et al.* Facile synthesis of FeCo@NC core–shell nanospheres supported on graphene as an efficient bifunctional oxygen electrocatalyst. Nano Res, 2017, 10: 2332–2343
31 Yang Y, Zhang W, Xiao Y, *et al.* $CoNiSe_2$ heteronanorods decorated with layered-double-hydroxides for efficient hydrogen evolution. Appl Catal B-Environ, 2019, 242: 132–139
32 Liang H, Gandi AN, Xia C, *et al.* Amorphous NiFe-OH/NiFeP electrocatalyst fabricated at low temperature for water oxidation applications. ACS Energy Lett, 2017, 2: 1035–1042
33 He K, Tadesse Tsega T, Liu X, *et al.* Utilizing the space-charge region of the FeNi-LDH/CoP p-n junction to promote performance in oxygen evolution electrocatalysis. Angew Chem Int Ed, 2019, 58: 11903–11909
34 Zhang H, Li X, Hähnel A, *et al.* Bifunctional heterostructure assembly of NiFe LDH nanosheets on NiCoP nanowires for highly efficient and stable overall water splitting. Adv Funct Mater, 2018, 28: 1706847
35 Chen L, He C, Wang R, *et al.* Potential active sites of Mo single atoms for electrocatalytic reduction of N_2. Chin Chem Lett, 2021, 32: 53–56
36 Sun T, Xu L, Wang D, *et al.* Metal organic frameworks derived single atom catalysts for electrocatalytic energy conversion. Nano Res, 2019, 12: 2067–2080
37 Chen L, Song Y, Liu Y, *et al.* NiCoP nanoleaves array for electrocatalytic alkaline H_2 evolution and overall water splitting. J Energy Chem, 2020, 50: 395–401
38 Zhang W, Li D, Zhang L, *et al.* NiFe-based nanostructures on nickel foam as highly efficiently electrocatalysts for oxygen and hydrogen evolution reactions. J Energy Chem, 2019, 39: 39–53
39 Niu S, Jiang WJ, Wei Z, *et al.* Se-doping activates FeOOH for cost-effective and efficient electrochemical water oxidation. J Am Chem Soc, 2019, 141: 7005–7013
40 Xu X, Song F, Hu X. A nickel iron diselenide-derived efficient oxygen-evolution catalyst. Nat Commun, 2016, 7: 12324
41 Wu T, Sun S, Song J, *et al.* Iron-facilitated dynamic active-site generation on spinel $CoAl_2O_4$ with self-termination of surface reconstruction for water oxidation. Nat Catal, 2019, 2: 763–772
42 He Q, Wan Y, Jiang H, *et al.* Nickel vacancies boost reconstruction in nickel hydroxide electrocatalyst. ACS Energy Lett, 2018, 3: 1373–1380
43 Asnavandi M, Yin Y, Li Y, *et al.* Promoting oxygen evolution reactions through introduction of oxygen vacancies to benchmark NiFe-OOH catalysts. ACS Energy Lett, 2018, 3: 1515–1520
44 Liu T, Li P, Yao N, *et al.* CoP-doped MOF-based electrocatalyst for pH-universal hydrogen evolution reaction. Angew Chem Int Ed, 2019, 58: 4679–4684
45 Yu L, Zhou H, Sun J, *et al.* Hierarchical Cu@CoFe layered double hydroxide core-shell nanoarchitectures as bifunctional electrocatalysts for efficient overall water splitting. Nano Energy, 2017, 41: 327–336
46 Lei Y, Shi Q, Han C, *et al.* N-doped graphene grown on silk cocoon-derived interconnected carbon fibers for oxygen reduction reaction and photocatalytic hydrogen production. Nano Res, 2016, 9: 2498–2509
47 Konkena B, Masa J, Botz AJR, *et al.* Metallic $NiPS_3$@NiOOH core-shell heterostructures as highly efficient and stable electrocatalyst for the oxygen evolution reaction. ACS Catal, 2017, 7: 229–237
48 Long X, Xiao S, Wang Z, *et al.* Co intake mediated formation of ultrathin nanosheets of transition metal LDH—an advanced electrocatalyst for oxygen evolution reaction. Chem Commun, 2015, 51: 1120–1123
49 Meng X, Han J, Lu L, *et al.* Fe^{2+}-doped layered double (Ni, Fe) hydroxides as efficient electrocatalysts for water splitting and self-powered electrochemical systems. Small, 2019, 15: 1902551
50 Bai X, Ren Z, Du S, *et al. In-situ* structure reconstitution of $NiCo_2P$ for enhanced electrochemical water oxidation. Sci Bull, 2017, 62: 1510–1518
51 Zhang FS, Wang JW, Luo J, *et al.* Extraction of nickel from NiFe-LDH into Ni_2P@NiFe hydroxide as a bifunctional electrocatalyst for efficient overall water splitting. Chem Sci, 2018, 9: 1375–1384
52 Gu C, Hu S, Zheng X, *et al.* Synthesis of sub-2 nm iron-doped $NiSe_2$ nanowires and their surface-confined oxidation for oxygen evolution catalysis. Angew Chem Int Ed, 2018, 57: 4020–4024
53 Jiang J, Sun F, Zhou S, *et al.* Atomic-level insight into super-efficient electrocatalytic oxygen evolution on iron and vanadium co-doped nickel (oxy)hydroxide. Nat Commun, 2018, 9: 2885
54 Gao Q, Zhang W, Shi Z, *et al.* Structural design and electronic modulation of transition-metal-carbide electrocatalysts toward efficient hydrogen evolution. Adv Mater, 2019, 31: 1802880
55 Yang Z, Liang X. Self-magnetic-attracted $Ni_xFe_{(1-x)}$@$Ni_xFe_{(1-x)}O$ nanoparticles on nickel foam as highly active and stable electrocatalysts towards alkaline oxygen evolution reaction. Nano Res, 2020, 13: 461–466
56 Wang Y, Liu Y, Liu W, *et al.* Regulating the coordination structure of metal single atoms for efficient electrocatalytic CO_2 reduction. Energy Environ Sci, 2020, 13: 4609–4624
57 Hsu SH, Miao J, Zhang L, *et al.* An earth-abundant catalyst-based seawater photoelectrolysis system with 17.9% solar-to-hydrogen efficiency. Adv Mater, 2018, 30: 1707261
58 Kuang Y, Kenney MJ, Meng Y, *et al.* Solar-driven, highly sustained splitting of seawater into hydrogen and oxygen fuels. Proc Natl Acad Sci USA, 2019, 116: 6624–6629

Acknowledgements This work was financially supported by Hunan Provincial Science and Technology Plan Project (2017TP1001 and 2020JJ4710), the National Key R&D Program of China (2018YFB0704100) and the State Key Laboratory Fund.

Author contributions Song C and Liu Y performed the experiments

and sample preparation; Song C and Wang Y wrote the paper with support from Lei Y; Tang S was responsible for the data processing; Li W and Zeng J contributed to the theoretical analysis; Li Q, Chen L and Peng H provided constructive suggestions. All authors contributed to the general discussion.

Conflict of interest The authors declare no conflict of interest.

Supplementary information Supporting data are available in the online version of the paper.

Chengye Song received his Bachelor degree from Jiangxi Science and Technology Normal University in 2016. He is currently pursuing his Master degree under the supervision of Prof. Yongpeng Lei and Prof. Wenkui Li.

Wenkui Li received his BS degree (1998) in Hebei University and Master degree (2001) in Hunan University, and his PhD degree (2004) in Shanghai Institute of Ceramics, Chinese Academy of Sciences with Prof. Hanrui Zhuang. He joined the faculty of Jiangxi Province Key Laboratory of Surface Engineering, Jiangxi Science & Technology Normal University in 2004 as a full professor.

Yongpeng Lei received his BS degree (2003) and Master degree (2006) in National University of Defense Technology, and his PhD degree (2011) in National University of Defense Technology with Prof. Yingde Wang. He started the study of functional nanomaterials at the Department of Chemistry, Tsinghua University in 2011, under the guidance of Prof. Yadong Li. He joined the faculty of the State Key Laboratory of Powder Metallurgy, Central South University in 2017 as a full professor.

层状镍铁双氢氧化物与金属磷化物耦合实现高效析氧和稳定的全解水

宋成叶[1,2†], 刘毅[1†], 王裕超[1,4†], 唐帅豪[1,5], 李文魁[2*], 李倩[1,4], 曾坚[1,5], 陈雷[3], 彭宏程[3], 雷永鹏[1,3,6*]

摘要 研制具有优良稳定性的高活性析氧反应(OER)电催化剂是一个巨大的挑战. 这项工作构建了层状镍铁双氢氧化物修饰的磷化物(NiFe LDH@CoP/NiP_3), 其在碱性介质中呈现出了令人满意的OER活性和良好的全解水稳定性. 在300 mV的过电位下, NiFe LDH@CoP/NiP_3的电流密度为82 mA cm^{-2}, 分别是CoP/NiP_3和NiFe LDH的9.1倍和2.3倍. 通过X射线光电子能谱、拉曼和扫描电镜表征, 研究了OER过程中的重构行为. 氢析出性能测试也论证了NiFe LDH与CoP/NiP_3之间的协同效应. 此外, NiFe LDH@CoP/NiP_3同时作为阴极和阳极进行全解水时, 可以维持100 mA cm^{-2}的高电流密度超过275小时. 此外, 在氙灯的照射下, 太阳能驱动的水分解可以实现9.89%的光产氢效率. 这项工作实现了不同活性成分间的耦合, 为双功能电催化剂的设计提供了参考.